Advances in Colloid and Interface Science 301 (2022) 102616

Contents lists available at ScienceDirect

Advances in Colloid and Interface Science

journal homepage: www.elsevier.com/locate/cis

Historical Perspective

Evaluation of noble metal nanostructure-serum albumin interactions in 2D and 3D systems: Thermodynamics and possible mechanisms

Ditta Ungor [a,b], Ádám Juhász [a,b], Norbert Varga [a,b], Edit Csapó [a,b,*]

[a] MTA-SZTE Lendület "Momentum" Noble Metal Nanostructures Research Group, University of Szeged, H-6720 Rerrich B. sqr. 1, Szeged, Hungary
[b] Interdisciplinary Excellence Center, Department of Physical Chemistry and Materials Science, University of Szeged, H-6720 Rerrich B. sqr. 1, Szeged, Hungary

ARTICLE INFO

Keywords:
Noble metals
Plasmonic nanoparticles
Fluorescent nanoclusters
Serum albumins
Binding affinities
Thermodynamics

ABSTRACT

In this review, we clearly highlight the importance of the detailed study of the interactions between noble metal colloids (nanoparticles (NPs) and nanoclusters (NCs)) with serum albumins (SAs) due to their rapidly growing presence in biomedical research. Besides the changes in the structure and optical property of SA, we demonstrate that the characteristic localized surface plasmon resonance (LSPR) feature of the colloidal noble metal NPs and the size- and structure-dependent photoluminescence (PL) property of the sub-nanometer sized NCs are also altered differently because of the interactions between them. Namely, for plasmonic NPs – SA interactions the PL quenching of SA (mainly static) is identified, while the SA cause PL enhancement of the ultra-small NCs after complexation. This review summarizes that the thermodynamic nature and the possible mechanisms of the binding processes are dependent partly on the size, morphology, and type of the noble metals, while the chemical structure as well as the charge of the stabilizing ligands have the most dominant effect on the change in optical features. In addition to the thermodynamic data and proposed binding mechanisms provided by three-dimensional spectroscopic techniques, the quantitative and real-time data of "quasi" two-dimensional sensor apparatus should also be considered to provide a comprehensive evaluation on many aspects of the particle/cluster – SA interactions.

1. Introduction

Noble metal nanostructures containing gold (Au), silver (Ag), or copper (Cu) are promising materials in the diverse field of science like chemistry, physics, biology, pharmacy as well as several medical uses (diagnostics, bio(sensing), imaging, therapy etc.) [1]. For their potential biomedical applications, the detailed understanding of the thermodynamic and kinetic features of the interactions between noble metal nanostructures (plasmonic nanoparticles (NPs) [2] or fluorescent sub-nanometer-sized nanoclusters (NCs)) [3] and plasma/serum proteins (SAs) is a key factor. The nature of the mentioned interactions such as coordination, hydrogen bonding, electrostatic or hydrophobic interactions, van der Waals forces, or steric hindrance is highly controllable by the size, morphology, surface functionalization, charge, and material quality of the metal structures, as well as the NPs/NCs–protein ratios, the pH and the incubation time, are also play an important role in the formation of these possible interactions [4–7]. Through the formation of the interactions the natural properties of both particles/clusters (e.g. optical features, aggregation etc.) and the proteins (e.g. secondary/tertiary structure, aggregation etc.) may be changed which can be easily followed by several physicochemical techniques like UV–Vis spectrophotometry, spectrofluorimetry, circular dichroism (CD) or Fourier-transformation infrared (FT-IR) and Raman spectroscopy, dynamic light scattering (DLS), electron microscopic images or two-dimensional (2D) measuring apparatus etc.

Several excellent articles can be found in the literature relating to the interpretation of the formation and the nature of the protein corona ("soft" or "hard" type) formed on the surface of particles [5,8–11], but this review exclusively focuses on the evaluations of the interactions between bovine (BSA) and human (HSA) serum albumins with plasmonic Au, Ag and Cu NPs and fluorescent Au, Ag and Cu NCs based on quantitative, thermodynamics, and kinetics aspects in 2D and 3D systems. We want to provide a comprehensive analysis of how the size, material quality, morphology, and the surface coatings of NPs ($d > 2$ nm) and NCs ($d < 2$ nm) affect the formation of interactions with proteins; how the optical properties of metals and the structure of proteins

* Corresponding author at: MTA-SZTE Lendület "Momentum" Noble Metal Nanostructures Research Group, University of Szeged, H-6720 Rerrich B. sqr. 1, Szeged, Hungary.
E-mail address: juhaszne.csapo.edit@med.u-szeged.hu (E. Csapó).

https://doi.org/10.1016/j.cis.2022.102616
Received 29 October 2021; Received in revised form 7 February 2022; Accepted 12 February 2022
Available online 15 February 2022

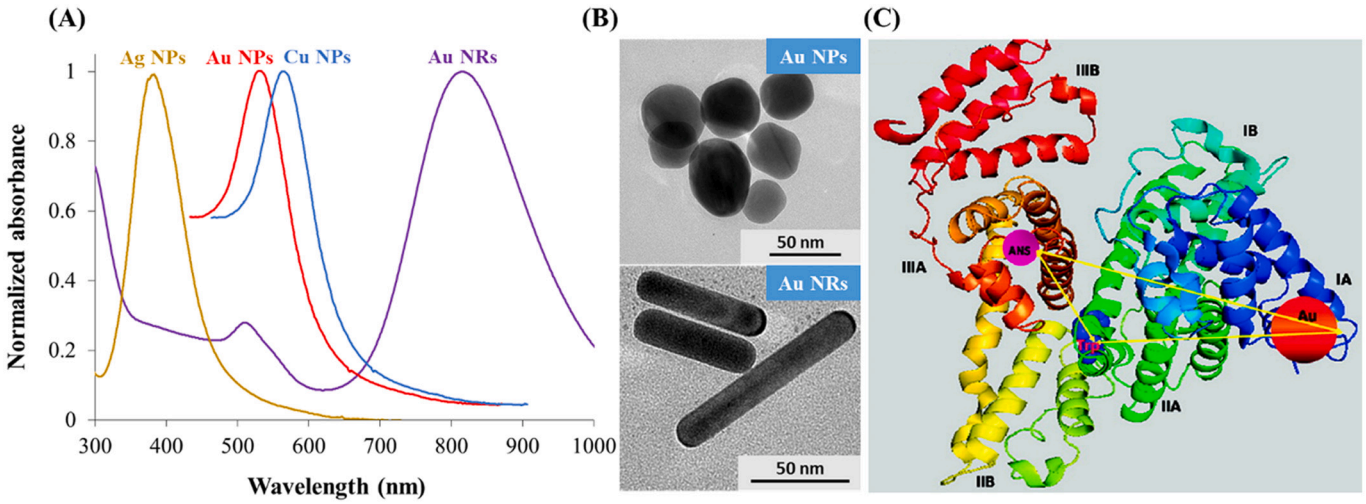

Fig. 1. (A) Localized surface plasmon resonance (LSPR) bands of spherical Ag, Au, Cu NPs, and rod-like Au nanoparticles (Au NRs) with (B) representative TEM images. (C) Schematic representation of a possible binding of an Au NP to HSA. Copyright (2011) ACS Publications. Used with permission from Ref. [27].

change. In contrast with the NPs, there are significantly fewer reports (ca. 3–4) on the interpretation of protein interactions with noble metal NCs [12,13] which possess several prominent features like well-defined molecular structure, discrete electronic transitions, and characteristic size-tunable PL. This review highlights and interprets the main differences and similarities of the interactions of SAs with metal nanostructures having different sizes and optical properties. The possibilities and benefits of the 2D techniques on the extract of the quantitative and real-time data of the NPs/NCs- SA interactions were also summarized.

Table 1
Interaction of different noble metal colloids with SAs: summary of the different structural parameters, conclusions of CD and FT-IR/Raman experiments, and the main thermodynamic data (if available) of the interactions calculated by the Stern-Volmer equation (n = number of binding sites; K_{SV} = Stern-Volmer constant (M^{-1}); ΔG° = Gibbs free energy (kJ mol^{-1}); ΔH° = enthalpy (kJ mol^{-1}); ΔS° = entropy (J mol^{-1} K^{-1}); *1 reduced by $NaBH_4$; *2 sonochemically synthesized).

Metal	Shape	Size (nm)	Surface stabilizer	Protein type	Type of PL quenching	Thermodynamics data	CD	FT-IR/ Raman	Ref
Cu	Spherical	7.5	-*1	BSA	Static	n ~ 1; $K_{SV} \sim 10^8$ M^{-1} (310*K*) $\Delta G^\circ < 0$ (− 44.5 kJ mol^{-1}) (310 K) $\Delta H^\circ > 0$ (62.3 kJ mol^{-1}) $\Delta S^\circ > 0$ (344.5 J mol^{-1} K^{-1})	Basic structure of the protein does not change	Basic structure of the protein does not change	[33]
Ag	Spherical	62	citrate	BSA	Static + dynamic	n ~ 1; $K_{SV} \sim 10^{-9}$ M^{-1} (301*K*) $\Delta G^\circ < 0$ (− 92.3 kJ mol^{-1}) (301 K) $\Delta H^\circ > 0$ (37.7 kJ mol^{-1}) $\Delta S^\circ > 0$ (396.8 J mol^{-1} K^{-1})	–	–	[32]
Au	Spherical	13	Citrate	BSA	Static	n ~ 1; $K_{SV} \sim 10^8$ M^{-1} (298 K)	Basic structure of the protein does not change	Basic structure of the protein does not change	[29]
			Cysteine		Static	n ~ 1; $K_{SV} \sim 10^8$ M^{-1} (298 K)			
			CTAB		Static	n ~ 2; $K_{SV} \sim 10^9$ M^{-1} (298 K)	Secondary structural changes occur	Secondary and tertiary structural changes occur	
			PEG (2 k)		Static	n ~ 1; $K_{SV} \sim 10^8$ M^{-1} (298 K)	Basic structure of the protein does not change	Basic structure of the protein does not change	
			PEG(5 k)		Static + dynamic	–			
Au	Spherical	16	Curcumin	HSA	Dynamic	n ~ 1; $K_{SV} \sim 10^4$ M^{-1} (308 K) $\Delta G^\circ < 0$ (− 24.8 kJ mol^{-1}) (308 K) $\Delta H^\circ > 0$ (35.5 kJ mol^{-1}) $\Delta S^\circ > 0$ (195.6 J mol^{-1} K^{-1})	Secondary no, but tertiary structural changes occur	–	[30]
Au	Spherical	16	Oleamide	HSA	Static	n ~ 1; $K_{SV} \sim 10^5$ M^{-1} (298 K) $\Delta G^\circ < 0$ (− 26.81 kJ mol^{-1})	–	–	[28]
Au	Spherical	16	PVP*2	BSA HSA	Static	n ~ 1; $K_{SV} \sim 10^4$ M^{-1} (298 K)	–	–	[31]

2. Noble metal nanoparticle – serum albumin interactions

Detailed studies of interactions between biologically important macromolecules (e.g. proteins) and colloidal particles (d = 2–30 nm) at solid/liquid interfaces have become increasingly dominant since the 1990s; several basic articles were published by Z. Adamczyk and his group [14–16]. In these works, numerous aspects like the random sequential adsorption (RSA) of spheroidal particles, several experimental and numerical simulations of the adsorption kinetics, the role of electrostatics double-layer interactions etc. have been summarized. Among colloidal particles, the noble metal-based particles (Au NPs, Ag NPs, Cu NPs) are in the focus of interest from the 2000s because of their excellent size- morphology- and composition-dependent optical features [1].

Namely, the noble metal particles having d > 2 nm in size show characteristic plasmonic features, because the collective oscillation of the free electron occurs. This optical property originates from the so-called localized surface plasmon resonance (LSPR) phenomena which results in the appearance of a characteristic plasmon band in the visible range of the electromagnetic spectrum (λ = 400–800 nm) (Fig. 1.A) [17,18]. This LSPR band can be tuned systematically with the size, morphology, and composition of NPs which are regulated by changing the synthesis conditions. For rod-like NPs [19,20] the tunability of LPSR to the near-infrared region (NIR) (Fig. 1.A) is extremely beneficial to overcome limited penetration of optical imaging systems achieve active penetration into tissues. The visible (VIS) and the NIR region with a wavelength ranging from 650 nm to 900 nm, referred to as the first "biological window", provides enhanced transparency to biological molecules and water. The noble metal NPs, especially Au NPs, are potential candidates in biomedical fields including, but not limited to imaging [21], (bio)sensing [22], diagnostics [23], therapy [2], or drug and gene delivery [24]. When these NPs are exposed to biological fluids, mainly proteins and other biomolecules are easily adsorbed onto the surface to form a protein "corona", which strongly depends on the size, morphology, composition, and surface functionalization of the NPs [5,8–10].

Several articles can be found in the literature relating to the evaluation of noble metal NPs - protein interactions based on several aspects. J. Simon et al. studied the modifications in nonlinear optical response and thermal diffusivity of BSA and HSA proteins induced by Au NPs [25], but the antibacterial properties of the mentioned protein-Au NPs complex were also investigated against several pathogens (e.g. *Bacillus pumilus, Escherichia coli, Staphylococcus aureus* etc.) [25]. It was found that the BSA/HSA-Au NPs combinations, containing citrate-stabilized spherical Au NPs having 13 nm in size, do not show antibacterial activity against the studied pathogens. A significant part of the publications is based on molecular dynamics calculations. Molecular simulations of Q. Shao et al. showed that even though the HSA protein remains in a folded structure, the presence of Au NPs (d = 4.0 nm) can cause more than 50% of the residues to decrease their flexibility significantly, and approximately 10% of the residues to change their secondary structure [26]. It was also reported previously by the work of T. Sen et al., that the Au NPs are attached to HSA by linkage through Cys53-Cys62 (Cys: cysteine) disulfide bond which is located at subdomain 1A of HSA confirmed by Surface Energy Transfer (SET) method, as the Fig. 1.C represents [27]. Their work also clearly highlights the importance of taking allosteric effects into account. The simulations suggested that allosteric effects must be considered when designing and applying NPs in medical and biological applications that depend on protein–NP interactions [27]. Because of the high importance of theoretical calculations, more specialized data can be found in Section 2.3.

In addition to these articles, a significant number of publications discuss the nature of PL quenching during the interaction of noble metal NPs with SAs as well as the thermodynamic parameters and proposed mechanisms of the quenching process, which is the main topic of this review. Table 1. summarizes some relevant articles which discuss the main thermodynamic data of the interactions of Au [28–31], Ag [32], and Cu [33] nanospheres with SAs calculated by the Stern-Volmer equation. Regardless of the quality of the noble metal colloids, the size, and type of surface-bounded ligands, a decrease in the fluorescence of the protein, i.e., PL quenching of the SA, occurs in all cases when noble metal NPs interact with SAs. The quenching mechanisms between SAs and plasmonic NPs are divided by static and dynamic types and this PL quenching mechanism may be evaluated using the Stern-Volmer eq. [28–31]. As Table 1. shows dominantly the static quenching can be obtained which supports the formation of a non-fluorescent complex between the albumins and the particles as quenchers. We can also state that the size of the NPs has no dominant effect on the number of binding sites (n), which is in almost every case $n = 1$. Based on articles published up to 2021 [28–33] the regardless of the quality of the metals, the interactions occur spontaneously ($\Delta G^\circ < 0$). Both ΔH° and ΔS° values are positive implying an endothermic process, which is entropy-driven. Moreover, both the positive values of ΔH° and ΔS° also suggest that the interaction forces are hydrophobic in nature.

The most marked difference is caused by the quality of the surface stabilizer molecules. Nor is the size of the molecules, much less its charge having a dominant effect on the nature of the interaction. G. Wang et al. presented in 2019 [29] that among the various surface-modified spherical Au NPs (stabilized by citrate-, Cys, polyethylene glycol (PEG) and cetyltrimethylammonium bromide (CTAB)) the CTAB-coated Au NPs having well-defined positive surface charge caused measurable conformational changes in the secondary structure of the SAs indicated that the surface charge of the NPs plays an important role in the interactions of SAs with noble metal colloids. It was also confirmed that the thickness of the protein coronas (ca. 3–13 nm) and the aggregation behaviors of different Au NPs are tightly related to the surface charge (e.g. Cys-Au NPs: ζ = −40.1 mV (thickness of corona = 13 nm); PEG(5 k)-Au NPs: ζ = −2.82 mV (thickness of corona = 2.5 nm)). Besides the type of the surface-bounded ligands, the morphology of the NPs may cause more significant changes in the protein structure. However, in Table 1., the main parameters of only spherical noble metal NPs–SA interactions are summarized, but G. Wang et al. published an article relating to the effects of Au NP morphologies on interactions with fibrinogen [34]. They found that compared to a spherical shape, the NPs having anisometric morphologies (rod/star) had the capacity to cause higher structural changes of the proteins confirmed by CD experiments. Among several spectroscopic techniques the combined use of CD and FT-IR or Raman techniques provide a comprehensive understanding of how protein structure changes because of the interaction with particles. For CD experiments the bands at 208 nm and 222 nm belongs to the characteristic signals of BSA or HSA produced by α-helical structure.

When proteins interact with NPs the intensity of these bands can decrease which resulting in change of the ratio of the secondary structural elements depending on the degree of the intensity change, while in case of Raman studies, the shift of the position as well as the intensity decrease of the amide-I (1600–1700 cm^{-1}), amide-II (1500–1600 cm^{-1}) and amide-III (1335–1340 cm^{-1}) peaks refer to same structural changes of the protein. The amide I band has contributions from different secondary structural elements, such as 1620–1645 cm^{-1} through β-sheet content, 1645–1652 cm^{-1} by random coil content, and 1652–1662 cm^{-1} by α-helix content. For example, for the formation of Cu NPs-BSA interaction [31] CD studies confirm the decrease of the helicity (α-helix content of the protein) from 52% to 47%, while the Raman data strongly confirm that the microenvironment around Trp is changed due to the interaction of Cu NPs. These results suggest the binding of Cu NPs to Trp fluorophore of BSA by forming ground state complex. Another article also confirms the similar conclusion of the experimental results of these two techniques in case of the study of the interaction of BSA with differently surface modified gold nanoparticles [27]. Among the citrate-, Cys-, PEG- and CTAB-coated Au NPs the positively charged CTAB-functionalized Au NPs cause measurable structural changes in the BSA conformation which is confirmed by the intensity changes of the above-

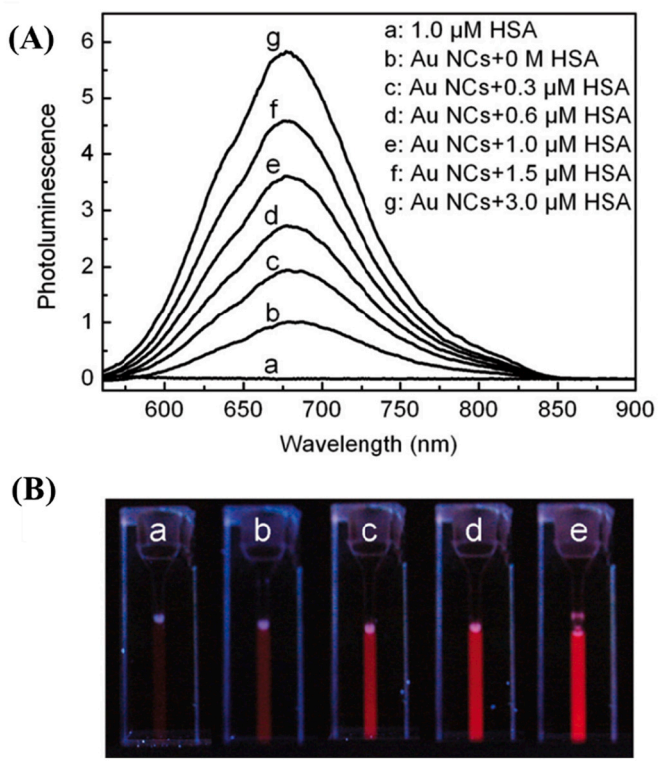

Fig. 2. (A) The PL spectra of red-emitting DHLA-Au NCs in the absence and the presence of HSA using different concentrations of HSA, $\lambda_{excitation} = 550$ nm (B) with the photos of the appropriate samples under UV-light, $\lambda_{lamp} = 360$ nm. Copyright (2012) Wiley-VCH GmbH. Used with permission from Ref. [49]. (For interpretation of the references to color in this figure legend, the reader is referred to the web version of this article.)

mentioned characteristic CD bands and amide bands in FT-IR spectra.

3. Noble metal nanocluster – serum albumin interactions

As it was mentioned in the *Introduction*, the ultra-small NCs are one of the most prominent nano-objects among the noble metal nanostructures. According to the generally accepted scientific views, they are defined based on their size and structural characteristic-originated optical properties. These small nano-objects contain only a few ten or hundred metal atoms; therefore, their size becomes comparable with the Fermi wavelength. This phenomenon causes the rupture of the continuous conductive band to discrete energy levels. Thus, the clusters show molecular-like behavior such as an intensive PL feature, which can easily tune with their size and the chemical structure of the surface ligands [35,36]. For the preparation of these ultra-small fluorescent noble metals, several routes are available. It can be stated that in the case of bottom-up strategies [37], the application of biomolecules (e.g. amino acids [38,39], nucleotides [40,41], proteins [42,43]) as a reducing and stabilizing agent is preferred for future biomedical uses. Furthermore, these biomolecules are applied directly as surface functionalizing agents as well. Several articles discuss the formation and exact structure of metal cluster cores in a protein cage [44–46]. Among these comprehensive works, Y. Xu et al. selected four model peptides (BSA, LYZ, trypsin, and pepsin) to analyze the different characteristics of the template molecules on the formation of fluorescent Au NCs [47]. Their work clearly presented that the positively charged amino acids of the selected proteins have a key role on the coordination of $AuCl_4^-$ to the protein chain. The tyrosine/tryptophane (Tyr/Trp) moieties reduce the precursor metal ions, while the Cys and histidine (His) residues are also important to stabilize the formed cluster cores. B. Maity and co-workers [48] also confirmed these findings for investigation of the nucleation of Au NCs in crystalline protein using theoretical calculations. They studied the ferritin as a model solid "bio-template", where the His49/Glu45/Arg52 (Glu: glutamate; Arg: arginine) cavity was a suitable cave for the cluster formation. While the Cd(II) ions, which integrated into the protein cage from the $(NH_4)_2SO_4/CdSO_4$ during the crystallization, served as an excellent seed for the Au NCs nucleation.

However, the formation of protein-directed Au NCs is a well-defined reaction, the direct interaction of SAs and noble metal NCs is discussed only to a negligible extent against the larger particles. The articles of L. Shang and G. U. Nienhaus are the most prominent works related to the dihydrolipoic acid (DHLA)-stabilized Au and Ag NCs [49–53]. They demonstrated firstly that the DHLA-Au [49] and DHLA-Ag NCs [50] have weak absorption in the visible light region, which originated the *sp to sp* and *d to sp* transitions.

The Au-based clusters show near-infrared emission at 684 nm using 550 nm excitation wavelength but the quantum yield (QY%) is very low value (< 1%). The average diameters are ca. 1.5 nm and 3.2 nm confirmed by HRTEM and DLS measurements, respectively. For the analysis of the binding between HSA and DHLA-Au NCs, classical steady-state fluorescence spectroscopy was applied. During investigations, it was determined that the emission intensity of the clusters is growing ca. 6-fold after the addition of 3.0 μM HSA, as Fig. 2. represents.

Moreover, the maximum of the emission wavelength was also shifted towards the blue region with 7 nm, which refers to the reduction of the local environment polarity due to the protein absorption. Based on the Hill evaluation of fluorescence spectra, the K_D and the n values were determined, which represent the strength of the interaction by equilibrium dissociation constant and the association cooperativity,

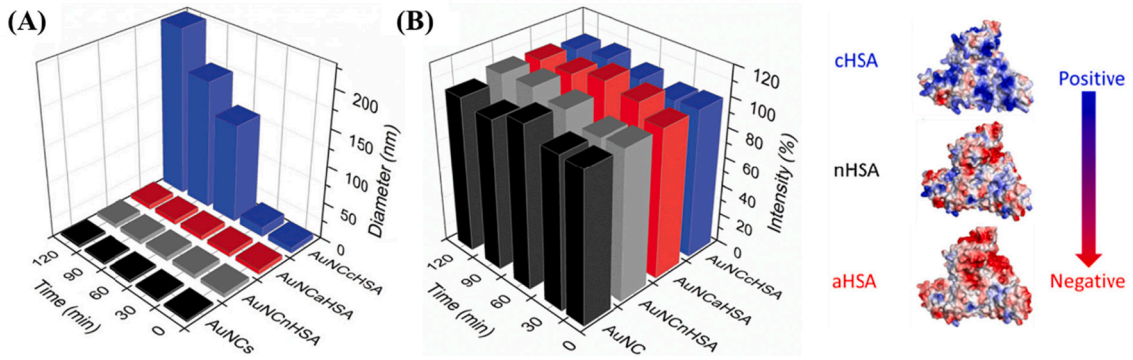

Fig. 3. (A) The hydrodynamic diameters and (B) the measured PL intensities of the studied DHLA-Au NCs – HSA complexes depending on the time with the schematic illustration of the HSA having various charges. Copyright (2013) Wiley-VCH GmbH. Used with permission from Ref. [51]. Copyright (2015) Elsevier. Used with permission from [52].

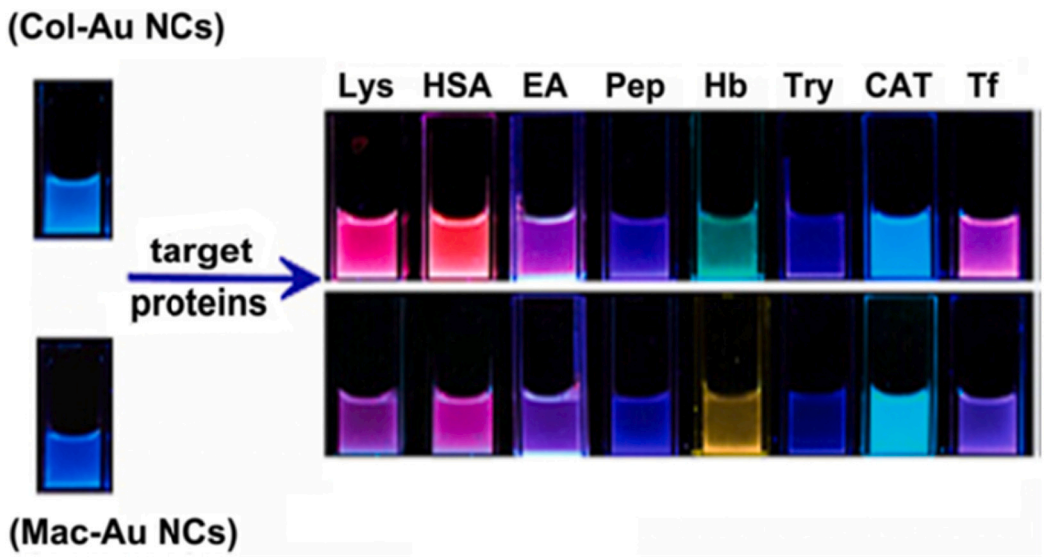

Fig. 4. The change of the PL of collagen (Col)-Au NCs and macerozyme (Mac)-Au NCs after the addition of different proteins under UV-light. Copyright (2014) ACS Publications. Used with permission from Ref. [57].

respectively. In the case of DHLA-Au NCs and HSA interaction, it was established that the strength of the interaction is comparable with larger NPs ($K_D = 0.9 \pm 0.1$ μM). Besides, the *n* is also larger than 1, which refers to the cooperative binding, where the affinity increases with the protein adsorption. To analyze the fluorescence decay profiles before and after the addition of HSA to DHLA-Au NCs, it was calculated that the origin 450 ns average lifetime became slower decay. This new 980 ns average lifetime origins from the shifts of the surface gold atom binding energies after the protein adsorption, which was also proved by XPS measurements. The interaction with HSA has been studied with DHLA-Ag NCs, as well. Choosing the 425 nm as excitation light source, the DHLA-Ag NCs show red emission at 630 nm. The QY% is better than the Au-based form, 2.4% was measured using sulforhodamine 101 as reference. The average size is 1.3 ± 0.3 nm, while the hydrodynamic diameter is 2.1 ± 0.4 nm. It was established that a two-fold fluorescence increasing was observed and the fluorescence lifetime was also changed in the presence of SA. The fluorescence lifetime of DHLA-Ag NCs is 5.6 ± 0.3 ns, which is modified with the presence of HSA to 6.8 ± 0.4 ns. Analyzing the PL properties of HSA by Stern-Volmer and Hill equation, it was evaluated that the emission of Trp214 was three-fold lower after the addition of Ag NCs. The magnitude of the determined K_D was in a similar range in the case of particle-protein interactions. In contrast, the characteristic CD spectrum of HSA was almost similar after the formation of a protein-cluster complex.

After modifying the charge of the HSA protein [51], it was also proved that the protein charge has a key role on the nature of the interaction. Namely, the positively charged cHSA shows a two-fold stronger affinity to the negatively charged DHLA-Au NCs. While the aHSA having negative charge binds ca. 15-fold weakly than the neutral HSA, which can be explained by the different magnitude of Coulomb forces in the case of various charged protein chains.

Nevertheless, these interactions can be easily tuned by ionic strength. To study the secondary structure of the HSA by CD spectrometry, it can be estimated that any significant change cannot be observed after the complexation of DHLA-Au NCs by neutral and negative HSA, while a fast and large-scale aggregation was identified in cHSA/DHLA-Au NCs complex (Fig. 3.).

In contrast to the DHLA-noble metal NCs, if the stabilizing ligand was changed to His amino acid, a combined fluorescence quenching of the blue-emitting NCs was observed during the steady-state fluorescence measurements of the interaction with BSA [54]. To analyze the PL spectra, it was determined that the quenching efficiency shows strong size-dependent because the calculated Stern-Volmer constants are 5-fold lower than in the case of plasmonic Au NPs. Based on the temperature effect, the thermodynamic parameters were also calculated. They proved that the interaction is thermodynamically favorable and hydrophobic force helps the contact between the cluster and protein. This π···π stacking of the aromatic amino acids of protein and imidazole ring of His was also supported by CD spectra, where the α-helix content of BSA was decreased from 54.3% to 35.2% after the interaction.

On the other hand, D. K. Sahu and K. Sahu proved in their work that the "naked" Cu NCs having blue emission at 430 nm do not cause any deficiency in the biological activity of BSA based on the negligible changes in secondary protein structure after the interaction [55]. The time-resolved fluorescence spectrometry pointed out that a Förster energy transfer (FRET) takes place between the Cu NCs-BSA, which decreases the Trp lifetime and increases the average τ value of Cu NCs by 3-fold as well.

The mentioned works demonstrated that the number of the exact studies is rather negligible related to the interaction between ultra-small NCs and SAs than it was presented for NPs, but for NCs, several application-oriented works can be found in the literature. The first article, which was written by Y. Wang et al., included the potential application of red-emitting Ag NCs ($\lambda_{em} = 656$ nm) for fluorescent imaging of SA in gel electrophoresis [56]. For the stabilizing, a polycytosine oligonucleotide template was applied, which generate a negative surface charge of the DNA-Ag NCs due to the phosphate-sugar backbone. Thus, the serum proteins have a positive charge at pH 3.4, the simple detection can be realized thanks to the electrostatic forces. The binding of HSA, the PL intensity of Ag NCs is drastically increased after 2 h, but the maximum value of the emission is decreased after 5 h due to the formation of large-scale cluster aggregates.

Besides the above-mentioned possibility, some articles can also be found, where multicolored sensor arrays were developed for identification not exclusively the SA [57–59]. S. Xu et al. synthesized two different blue-emitting Au NCs stabilized by collagen (Col) and macerozyme (Mac), which can produce a spectacular color change (Fig. 4.) in the emission wavelength depending on the nature of the identified proteins (lysozyme (Lys), human serum albumin (HSA), egg white albumin (EA), pepsin (Pep), hemoglobin (Hb), trypsin (Try), catalase (CAT), transferrin (Tf)). They established that Au NCs bind exothermically in the hydrophobic sites on the proteins by hydrophobic forces, while the folded structure of the proteins is also destroyed by the interaction. The lifetimes of the Au NCs are increased, and the maxima

of emission show red shifts due to the partial reoxidation of Au^0 to Au^+ and formation of thiol–Au(I) complex on the surface after the protein adsorption.

The research group of Wei Chen widely investigates the biomedical, especially sensor applications of various Au NCs. In their work, they firstly demonstrated the 6-aza-2-thio-thymine-stabilized Au NCs (ATT-Au NCs) as a potential BSA sensor [60], where the green emission intensity of ATT-Au NCs increased more than 13-fold after the SA binding. Based on the temperature-dependent PL measurements, the nature of the binding process was also calculated, where the positive enthalpy and entropy change refers to the hydrophobic forces between the nucleobases and the aromatic side chains of amino acids in BSA.

A. Akhuli et al. studied the interactions of Cu NCs with BSA with fluorescence correlation spectroscopy (FCS), isotherm titration calorimetry (ITC), and ζ-potential studies [61]. For stabilization of the NCs, tannic acid (TA), chitosan (Chit), and Cys amino acid were applied; the stabilized NCs have ca. 2.3 nm average diameter by TEM. Using 360 nm as excitation wavelength, the TA-Cu NCs, the Chit-Cu NCs, and the Cys-Cu NCs show 430, 432, and 490 nm emission wavelength, respectively. The fluorescence intensity of all three Cu clusters increases after the complexation of BSA. In the case of TA- and Chit-Cu NCs, the 1:1/NCs: BSA stoichiometry was observed due to the good linear correlation of $1/(F—F_0)$ vs reciprocal of the protein concentration function, while a multiple binding was assumed between Cys-Cu NCs and BSA. Moreover, the decay profiles were also changed, a systematic increase of the measured lifetimes was identified in the presence of the protein. Based on the DLS measurements, it was estimated that the formed BSA layer is smaller than a complex protein corona thickness on a classical particle. Based on the experimental results they proposed that the clusters adsorb onto the surface of an individual protein molecule instead of the protein adsorption on a metal surface. The study of the change in the fluorescence of BSA after the interaction with Cu NCs shows that all clusters cause quenching in the PL of protein by two different mechanisms depending on the metal concentration. For small concentrations, a static quenching was observed dominantly based on the determined quenching constants, while in the case of larger NC concentration the fluorescence lifetime of BSA was decreased, which proved a dynamic process.

Besides SAs, several great works can be found in the literature about the evaluation of other protein–NCs interactions, which are not currently covered by this comprehensive work. Without the claiming of completeness, an interesting manuscript can be read about the interaction of fluorescent nano metals and MPT63 protein [62], application as immunoassay for the detection of a-fetoprotein [63], aggregation process by insulin and γ-globulin immunoprotein [64], as well as the detection of human papillomavirus E6 protein by DNA-Ag NCs [65].

In summary, it can be estimated that if the stabilizing ligand of the synthesized NCs has electron-rich atoms or moieties (e.g. -COOH, $-NH_2$), the *p* orbitals from the surface ligands can easily overlap with the adjacent *O* or *S* atoms in proteins, which can activate the luminescent sites of cluster surface. Generally, this interaction can be supported by the hydrophobic forces, which can be realized by aromatic surface ligands and amino acids in a protein having aromatic side chains. Besides, the aggregation-induced emission (AIE) can also facilitate the enhancement of the fluorescence by the inhibited intramolecular rotations and vibrations.

4. Theoretical simulation in studying the interactions between noble metal nanostructures and serum proteins

Addition of noble metal NPs and NCs into the bloodstream leads to the creation of a solid/liquid interface where dynamic interactions between the solid surfaces of nano-object and blood components take place. Considering the particle size and the strongly curved surface is a common consequence the formation of the protein corona, what is a network of self-assembled proteins, and that new semi-solid biomimetic surface can sharply alter the properties of the nanoparticle. This biomimetic surface can lead to substantial divergences from the projected cellular uptake as well as biological responses. Peptide coating can not only ensure biocompatibility upon nano-sized particles, but also provides with specific functionalities as far as the transportation of Au NPs and NCs through cell membrane. Reaching a deeper understanding of the nano–object and biomolecule created interface is still challenging due to the synergistic effects of numerous manipulating factors (pH, ionic strength, hydrophobic effects etc.). Because of the complexity of these hybrid nanomaterials, modeling approaches at a molecular level represent the ideal tools for a detailed understanding of the governing forces and processes at the nano–bio interface.

MD simulations have been frequently used to discover the properties of biofunctionalized Au NPs. For example, for alkanethiol-type ligands, asymmetric allocation on gold substrates is preferred, resulting in anisotropic self-assembly on the mesoscale [66], and adsorption to lipid bilayers and degradation of the bilayer structure have also been characterized [67]. Modifying of self-assembly properties and structural changes of DNA-covered Au NPs have also been investigated using MD techniques, as well as the influence of DNA coatings on their interactions with cell membranes [68]. Despite the widespread applicability of peptide-coated Au NPs and NCs, to our knowledge there is a relatively small amount of computational data for these peptide-coated and especially SA-coated systems. The topic of the study of the interactions between Au NPs and proteins is limited in this work to bare or “small” molecule covered NPs [26,27,69] and disregarding the details of the interaction between protein-coated Au NPs and proteins [70].

Due to the aforementioned widespread application of Au NPs, especially in medicine, the docking of HSA to Au NPs has been investigated via MD simulation by Ramezani et al. [71]. In this theoretical study the helix structure of adsorbed HSA, such as length-, dipole-, radius- of helix as well as the length of hydrogen bonds, were estimated. Results of simulation indicated that sorption of protein on the Au NPs modifies the hydrophobic space between the alpha helix, and then the conditions for the entry of water into the protein are provided in this way primary denaturation occurs.

Tavanti and Menziani studied the interaction of four common blood proteins, including SA, with hydrophobic 11-mercapto-1-undecanesulfonate (MUS) covered Au NPs by MD method [72]. The object of the research was to gain quantitative insight into the kinetics of the interaction, the physicochemical properties of the binding site and the adsorption capacity of the NPS. Simulations have shown that SA bind to MUS-terminating AuNPs through hydrophobic interactions, and this adapt to Au surfaces to increase area, but in contrast to previous mentioned study [71], dramatic transformation in the secondary structure of proteins was not observed.

Therefore, it cannot be ignored that in the case of functionalized and bare particles, the interaction in terms of protein structure may be completely different. Furthermore, it should be noted that in these models, the particle size of NPs is nearly equal or larger than the average diameter of the protein. Radically different results are expected for NCs that are small enough to reach the interior part of the protein. Russell et al. investigated the location of Au NCs within bovine serum albumin (BSA) combining MD simulations and fluorescence spectroscopic measurements [73]. Outcomes of MD simulations demonstrated that the gold NCs growing close to the cysteine sites within all three domains of BSA. Besides, only two domains (IIB and IA) were found to accommodate large NCs containing more than 12 atoms.

The importance of all these simulations stems from the fact that an understanding of the exact orientation of Au NPs and NCs is essential for any future work that seeks to exploit the plasmonic and fluorescent properties of these hybrid materials.

5. Two-dimensional studies at solid/liquid interface

In previous chapters (2.1 and 2.2), it was summarized, that based on the experimental results of mainly spectroscopic techniques, we can

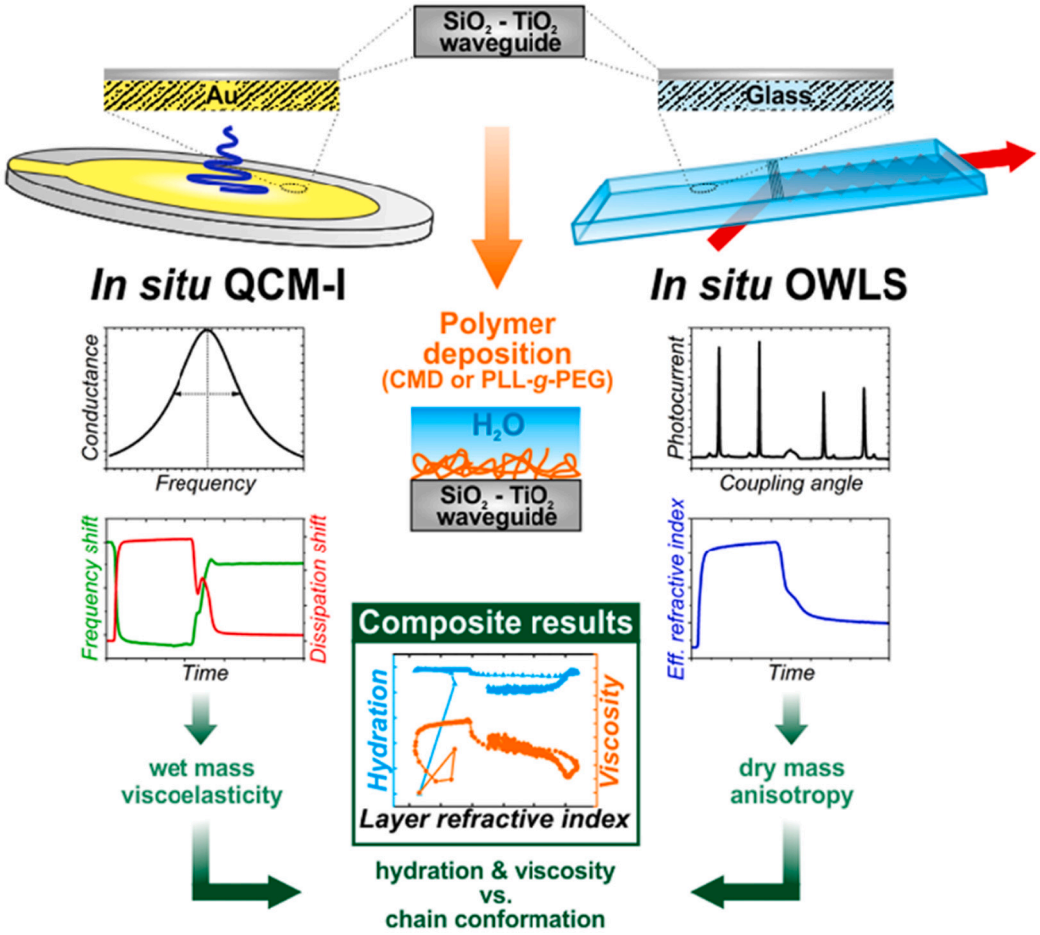

Fig. 5. Schematic representation of the advantages of the combination of QCM and OWLS for detailed structural analysis of the adsorbed macromolecules at solid/liquid interfaces. Copyright (2018) Nature Publications. Used with permission from Ref. [87].

provide information on the nature of noble metal NPs/NCs-SA interactions (through main thermodynamic parameters and the proposed mechanisms), but quantitative and real-time data cannot be given on the sorption properties, the structure of the adsorption layer and the kinetic characteristics of the emerging interactions. It is indisputable that several real-time and equilibrium analysis techniques are available that can be used to observe and quantify the mentioned sorption processes [74,75]. For example, the radiolabeled methods with strong scientific background are reproducible and rapid techniques [76], but they carry some disadvantages being that they are dangerous to human health; produce radioactive waste, and require special laboratory conditions. Perhaps this was one of the biggest motivations that led to the development of "label-free" assays based on optical methods. To determine these essential data, various two-dimensional (2D) measurement techniques, such as atomic force microscopy (AFM) [77] surface plasmon resonance (SPR) spectroscopy [78,79], optical waveguide light mode spectroscopy (OWLS) [80], or quartz crystal microbalance (QCM) [81,82], are excellently applicable. In addition to all these, there are really promising examples of combined techniques in the mentioned topic such as AFM and ellipsometry (ELM) - [83], AFM and SPR- [84], time-of-flight secondary-ion mass spectrometry (ToF-SIMS), and OWLS [85] coupled investigations. There is a serious potential of multi-technique applied approaches that can study the change in sorption processes as a function of time and temperature.

Based on the possibilities offered by 2D techniques, F. Höök et al. have been studied and compared the adsorption kinetics of three model proteins (HSA, fibrinogen, and Hb) using three different experimental techniques OWLS, ELM, and QCM [86]. The difference between the physical fundamentals of the applied methods is at least as important as the possibility of real-time studies (Fig. 5). While OWLS is sensitive to changes in the refractive index in the evanescent field thus, it measures the "non-solvated" amount of the adsorbed layer, whereas the QCM oscillations drag every molecule below the shear-plane and as such measure the hydrated mass of the adsorbed macromolecules (Fig. 5.) [88]. Thanks to the above-mentioned fast, small sample-demand, and variable techniques, the interaction between gold film-coated sensor surface, which can be modeling the surface of noble metal NPs, and the studied SAs can be characterized at solid/liquid interface [89,90]. Z. Adamczyk et al. studied the adsorption kinetics of HSA on a gold-coated QCM sensor surface at pH = 3.5 medium using different ionic strengths and bulk concentrations [91]. The studies have shown that the roughness of the sensor surfaces significantly affects the QCM-determined kinetic results. In addition, it has been demonstrated that the adsorption of HSA changes linearly at the low surface coverage region, where the slope is significantly influenced by the bulk HSA concentration. For the rougher gold sensor ((root mean square) rms = 2.5 nm; (average roughness height) $h_c = 6$ nm; flow medium: pH 3.5, $c_{NaCl} = 0.15$ M, flow rate 2.5×10^{-3} cm^3 s^{-1}), the mass transfer rate constant, the water factor and the hydration function were much smaller at $t < 20$ s than in case of their previous results of the silica sensor (sensor surface: rms = 0.86 nm, hc = 2 nm) [92]. It is important to note that the hydration function determined at the gold sensor increases with HSA coverage and it is significantly influenced by the ionic strength of the medium. Scott B. Thourson et al. studied the adsorption properties of BSA on the *N*-hydroxysuccinimide-functionalized and the non-functionalized QCM gold sensors [93], where it was found that regardless of the used surface,

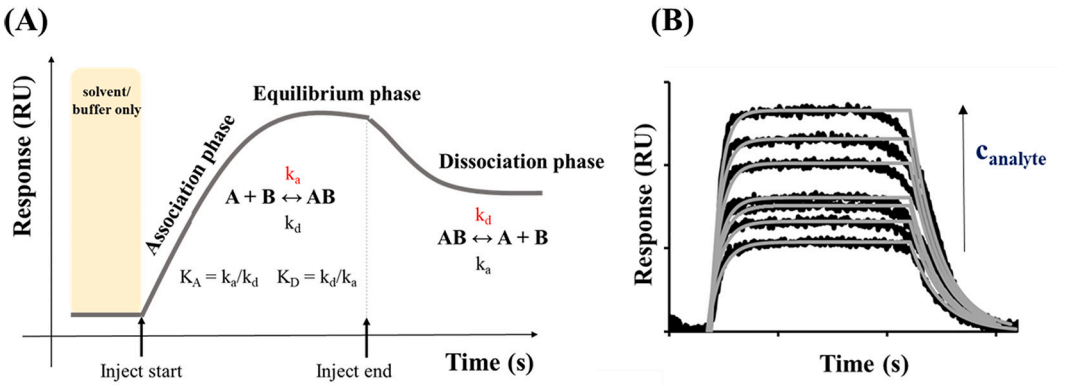

Fig. 6. (A) Determination of the real-time kinetic parameters (association (k_a) and dissociation (k_d) rate constants) of a studied system by using an SPR sensorgram. (B) Representative SPR sensorgram series at different analyte concentrations.

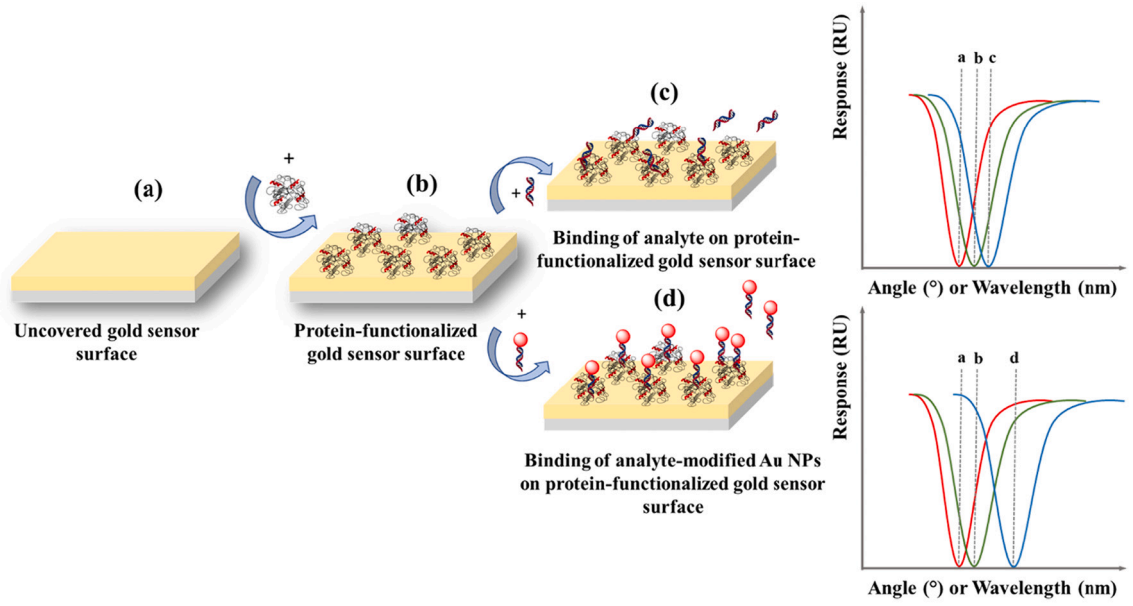

Fig. 7. Schematic representation of the detection of an analyte having low concentration by using 2D SPR technique without (c) and with (d) the application of plasmonic Au NPs.

the BSA saturation was 450 ± 26 ng cm^{-2} (pH = ~ 7.6), which can be explained in both cases by a large number of binding sites relative to the size of the protein. In a later work, E. Csapó et al. proved by SPR technique, that after the rinsing phase, which is caused the desorption of the reversibly bound BSA, the amount of BSA bound on the gold surface was $m^s_{pH=7.4}$ = 86.0 ng cm^{-2} and $m^s_{pH=3.0}$ = 56.5 ngcm^{-2} at pH = 7.4 and pH = 3.0, respectively [90]. Using a previous calculation procedure [94], it was found, the BSA has a larger cross-sectional area at lower pH values, which confirmed, that the changing of the pH-dependent secondary structure of the BSA was affected the adsorption processes. Based on the experiments in different pH and apparent potential surfaces, Burcu Beykal et al. showed, that the amount of adsorbed protein increases significantly in the case of the oppositely charged protein and gold electrode surface, which can be further increased by increasing the potential [95]. For the latter mentioned 2D SPR techniques, every small refractive index change related to the immobilized species on the surface of the gold sensor chip can be detected in the form of response unit (RU) signals (Fig. 6.A). The variation in the refractive index created by the capture of molecules depends on the concentration of analyte (Fig. 6.B) at the evanescent fields of the sensor and the properties of the target molecules/NPs [96,97]. Fig. 6.A shows a representative SPR sensorgram, which represents the determination possibilities of the real-time kinetic parameters (association (k_a) and dissociation (k_d) rate constants) of the studied system. If the measurements have been carried out at different analyte concentrations (as the Fig. 6.B summarizes) and various temperatures besides the mentioned kinetic parameters, the main thermodynamic functions, like Gibbs free energy, enthalpy and entropy changes can be obtained.

Nanosized noble metal (primarily gold) nanoobjects (NOs) are successful enhancers in ultra-sensitive SPR-based biosensors [98]. The use of SPR methods is limited to the detection of low concentrations [99] and/or low molecular weights [99] of analytes due to the smaller refractive index change by the sorption on the sensor surface. Hence, enhancing procedures using metal NOs can cause a more characteristic shift in SPR response, as the Fig. 7 represents, because of intensifying the refractive index change. Usually, a "sandwich" structure [98] is applied (e.g. gold sensor surface/BSA/Au NPs) in order to bind the analyte specifically to an aptamer with high density and thus high specific mass tags like spherical Au NPs [99–104], Au NRs [105–108], nanostars (Au NSs) [109] and nanocages [110]. The interactions between SA and noble metal NPs can be influenced by many factors, knowledge of which are essential for the characterization of the systems. The effect of each parameter is not fully known, so there is great research potential to examine these.

6. Conclusion

Nanoparticles are key components of modern nanotechnology developments in both material and life sciences in the 21st century. Among the large variety of nanoparticle types, the Au, Ag and Cu NPs/NCs have unique size-, shape- and composition-dependent optical, electric, and magnetic features which properties are strongly dependent upon methods to synthesize, purify, and characterize them. Detailed investigations of noble metal nanostructure–SA interactions play an increasingly important role in medical applications, like imaging, sensing, diagnostics, therapy, drug, and gene delivery as well. The noble metal NPs and NCs possess different size-, and structure-dependent optical features, which change differently by albumin-binding. To the best of our knowledge as well as according to the articles published till 2021, in this review, we summarized all the works related to the direct investigation of only SAs with noble metal NPs and NCs. It was established, while the classic plasmonic NPs cause dominantly the quenching of SA emission, the complexation between the mentioned proteins and the NCs results in the enhancement of NCs fluorescence mainly. Because the number of articles for interpretation of SA – NCs binding is relatively few, there is a growing demand to study these systems as well. It was also highlighted that the combination of 2- and 3-dimensional techniques gives more overall data (quantitative, thermodynamic, kinetic) on these important interactions.

CRediT authorship contribution statement

Ditta Ungor: Conceptualization, Writing – original draft. **Ádám Juhász:** Visualization, Writing – original draft. **Norbert Varga:** Visualization, Writing – original draft. **Edit Csapó:** Conceptualization, Resources, Supervision, Writing – original draft, Writing – review & editing.

Declaration of Competing Interest

The authors declare that they have no known competing financial interests or personal relationships that could have appeared to influence the work reported in this paper.

Acknowledgement

Project no. TKP2021-EGA-32 has been implemented with the support provided by the Ministry of Innovation and Technology of Hungary from the National Research, Development and Innovation Fund, financed under the TKP2021-EGA funding scheme. This research was also supported by the NRDIO through FK131446, PD137938 and PD142143 projects. The publication was also funded by the University of Szeged Open Access Fund (Grant No. 5660). Á. Juhász thanks the financial support of the ÚNKP-21-4-SZTE-516 new National Excellence Program of the Ministry for Innovation and Technology from the source of the NRDIF. This work is supported by the János Bolyai Research Fellowship of the Hungarian Academy of Sciences.

References

[1] Dykman L, Khlebtsov N. Gold nanoparticles in biomedical applications: recent advances and perspectives. Chem Soc Rev 2012;41:2256–82. https://doi.org/10.1039/c1cs15166e.
[2] Huang X, El-Sayed MA. Gold nanoparticles: optical properties and implementations in cancer diagnosis and photothermal therapy. J Adv Res 2010;1:13–28. https://doi.org/10.1016/j.jare.2010.02.002.
[3] Zheng Y, Lai L, Liu W, Jiang H, Wang X. Recent advances in biomedical applications of fluorescent gold nanoclusters. Adv Colloid Interf Sci 2017;242:1–16. https://doi.org/10.1016/j.cis.2017.02.005.
[4] Wang P, Wang X, Wang L, Hou X, Liu W, Chen C. Interaction of gold nanoparticles with proteins and cells. Sci Technol Adv Mater 2015;16:34610. https://doi.org/10.1088/1468-6996/16/3/034610.
[5] García-Álvarez R, Hadjidemetriou M, Sánchez-Iglesias A, Liz-Marzán LM, Kostarelos K. In vivo formation of protein corona on gold nanoparticles. the effect of their size and shape. Nanoscale 2018;10:1256–64. https://doi.org/10.1039/c7nr08322j.
[6] Barbir R, Capjak I, Crnković T, Debeljak Ž, Domazet Jurašin D, Ćurlin M, et al. Interaction of silver nanoparticles with plasma transport proteins: a systematic study on impacts of particle size, shape and surface functionalization. Chem Biol Interact 2021;335:109364. https://doi.org/10.1016/j.cbi.2020.109364.
[7] Sousa AA, Schuck P, Hassan SA. Biomolecular interactions of ultrasmall metallic nanoparticles and nanoclusters. Nanoscale Adv 2021;3:2995–3027. https://doi.org/10.1039/d1na00086a.
[8] Piloni A, Wong CK, Chen F, Lord M, Walther A, Stenzel MH. Surface roughness influences the protein corona formation of glycosylated nanoparticles and alter their cellular uptake. Nanoscale 2019;11:23259–67. https://doi.org/10.1039/c9nr06835j.
[9] Lai W, Wang Q, Li L, Hu Z, Chen J, Fang Q. Interaction of gold and silver nanoparticles with human plasma: Analysis of protein corona reveals specific binding patterns. Colloids Surf B: Biointerfaces 2017;152:317–25. https://doi.org/10.1016/j.colsurfb.2017.01.037.
[10] del Pilar Chantada-Vázquez M, López AC, Bravo SB, Vázquez-Estévez S, Acea-Nebril B, Núñez C. Proteomic analysis of the bio-corona formed on the surface of (Au, Ag, Pt)-nanoparticles in human serum. Colloids Surf B: Biointerfaces 2019;177:141–8. https://doi.org/10.1016/j.colsurfb.2019.01.056.
[11] Singh N, Marets C, Boudon J, Millot N, Saviot L, Maurizi L. In vivoprotein corona on nanoparticles: does the control of all material parameters orient the biological behavior? Nanoscale Adv 2021;3:1209–29. https://doi.org/10.1039/d0na00863j.
[12] Yin MM, Dong P, Chen WQ, Xu SP, Yang LY, Jiang FL, et al. Thermodynamics and mechanisms of the interactions between ultrasmall fluorescent gold nanoclusters and human serum albumin, γ-globulins, and transferrin: a spectroscopic approach. Langmuir 2017;33:5108–16. https://doi.org/10.1021/acs.langmuir.7b00196.
[13] Yin MM, Chen WQ, Lu YQ, Han JY, Liu Y, Jiang FL. A model beyond protein corona: Thermodynamics and binding stoichiometries of the interactions between ultrasmall gold nanoclusters and proteins. Nanoscale 2020;12:4573–85. https://doi.org/10.1039/c9nr09170j.
[14] Adamczyk Z. Kinetics of diffusion-controlled adsorption of colloid particles and proteins. J Colloid Interface Sci 2000;229:477–89. https://doi.org/10.1006/jcis.2000.6993.
[15] Adamczyk Z, Weroński P. Random sequential adsorption on partially covered surfaces. J Chem Phys 1998;108:9851–8. https://doi.org/10.1063/1.476423.
[16] Adamczyk Z, Warszyński P. Role of electrostatic interactions in particle adsorption. Adv Colloid Interf Sci 1996;63:41–149. https://doi.org/10.1016/0001-8686(95)00281-2.
[17] Majzik A, Fülöp L, Csapó E, Bogár F, Martinek T, Penke B, et al. Functionalization of gold nanoparticles with amino acid, β-amyloid peptides and fragment. Colloids Surf B: Biointerfaces 2010;81:235–41. https://doi.org/10.1016/j.colsurfb.2010.07.011.
[18] Csapó E, Patakfalvi R, Hornok V, Tóth LT, Sipos Á, Szalai A, et al. Effect of pH on stability and plasmonic properties of cysteine-functionalized silver nanoparticle dispersion. Colloids Surf B: Biointerfaces 2012;98:43–9. https://doi.org/10.1016/j.colsurfb.2012.03.036.
[19] Pérez-Juste J, Pastoriza-Santos I, Liz-Marzán LM, Mulvaney P. Gold nanorods: Synthesis, characterization and applications. Coord Chem Rev 2005;249:1870–901. https://doi.org/10.1016/j.ccr.2005.01.030.
[20] Kálomista I, Kéri A, Ungor D, Csapó E, Dékány I, Prohaska T, et al. Dimensional characterization of gold nanorods by combining millisecond and microsecond temporal resolution single particle ICP-MS measurements. J Anal At Spectrom 2017;32:2455–62. https://doi.org/10.1039/c7ja00306d.
[21] Wu Y, Ali MRK, Chen K, Fang N, El-Sayed MA. Gold nanoparticles in biological optical imaging. Nano Today 2019;24:120–40. https://doi.org/10.1016/j.nantod.2018.12.006.
[22] Zeng S, Yong KT, Roy I, Dinh XQ, Yu X, Luan F. A review on functionalized gold nanoparticles for biosensing applications. Plasmonics 2011;6:491–506. https://doi.org/10.1007/s11468-011-9228-1.
[23] Zhou W, Gao X, Liu D, Chen X. Gold nanoparticles for in vitro diagnostics. Chem Rev 2015;115:10575–636. https://doi.org/10.1021/acs.chemrev.5b00100.
[24] Ghosh P, Han G, De M, Kim CK, Rotello VM. Gold nanoparticles in delivery applications. Adv Drug Deliv Rev 2008;60:1307–15. https://doi.org/10.1016/j.addr.2008.03.016.
[25] Simon J, Udayan S, Nampoori VPN, Kailasnath M. Investigations on nonlinear optical properties and thermal diffusivity of gold nanoparticle embedded protein complex. Opt Laser Technol 2021;138:106859. https://doi.org/10.1016/j.optlastec.2020.106859.
[26] Shao Q, Hall CK. Allosteric effects of gold nanoparticles on human serum albumin. Nanoscale 2017;9:380–90. https://doi.org/10.1039/c6nr07665c.
[27] Sen T, Mandal S, Haldar S, Chattopadhyay K, Patra A. Interaction of gold nanoparticle with human serum albumin (HSA) protein using surface energy transfer. J Phys Chem C 2011;115:24037–44. https://doi.org/10.1021/jp207374g.
[28] Anand K, Rajamanikandan R, Selva Sharma A, Ilanchelian M, Khan FI, Tiloke C, et al. Human serum albumin interaction, in silico and anticancer evaluation of Pine-Gold nanoparticles. Process Biochem 2020;89:98–109. https://doi.org/10.1016/j.procbio.2019.09.036.
[29] Wang G, Yan C, Gao S, Liu Y. Surface chemistry of gold nanoparticles determines interactions with bovine serum albumin. Mater Sci Eng C 2019;103. https://doi.org/10.1016/j.msec.2019.109856.

[30] Foo YY, Kabir MZ, Periasamy V, Malek SNA, Tayyab S. Spectroscopic studies on the interaction of green synthesized-gold nanoparticles with human serum albumin. J Mol Liq 2018;265:105–13. https://doi.org/10.1016/j.molliq.2018.05.115.
[31] Naveenraj S, Anandan S, Kathiravan A, Renganathan R, Ashokkumar M. The interaction of sonochemically synthesized gold nanoparticles with serum albumins. J Pharm Biomed Anal 2010;53:804–10. https://doi.org/10.1016/j.jpba.2010.03.039.
[32] Mariam J, Dongre PM, Kothari DC. Study of interaction of silver nanoparticles with bovine serum albumin using fluorescence spectroscopy. J Fluoresc 2011;21:2193–9. https://doi.org/10.1007/s10895-011-0922-3.
[33] Bhogale A, Patel N, Mariam J, Dongre PM, Miotello A, Kothari DC. Comprehensive studies on the interaction of copper nanoparticles with bovine serum albumin using various spectroscopies. Colloids Surf B: Biointerfaces 2014;113:276–84. https://doi.org/10.1016/j.colsurfb.2013.09.021.
[34] Wang G, Wang W, Shangguan E, Gao S, Liu Y. Effects of gold nanoparticle morphologies on interactions with proteins. Mater Sci Eng C 2020;111:110830. https://doi.org/10.1016/j.msec.2020.110830.
[35] Zheng J, Zhou C, Yu M, Liu J. Different sized luminescent gold nanoparticles. Nanoscale 2012;4:4073. https://doi.org/10.1039/c2nr31192e.
[36] Yang TQ, Peng B, Shan BQ, Zong YX, Jiang JG, Wu P, et al. Origin of the photoluminescence of metal nanoclusters: from metal-centered emission to ligand-centered emission. Nanomaterials 2020;10:1–24. https://doi.org/10.3390/nano10020261.
[37] Ungor D, Dékány I, Csapó E, et al. Reduction of tetrachloroaurate(Iii) ions with bioligands: Role of the thiol and amine functional groups on the structure and optical features of gold nanohybrid systems. Nanomaterials 2019;9:1229. https://doi.org/10.3390/nano9091229.
[38] Csapó E, Ungor D, Juhász Á, Tóth GK, Dékány I. Gold nanohybrid systems with tunable fluorescent feature: Interaction of cysteine and cysteine-containing peptides with gold in two- and three-dimensional systems. Colloids Surfaces A Physicochem Eng Asp 2016;511:264–71. https://doi.org/10.1016/j.colsurfa.2016.10.003.
[39] Csapó E, Ungor D, Kele Z, Baranyai P, Deák A, Juhász Á, et al. Influence of pH and aurate/amino acid ratios on the tuneable optical features of gold nanoparticles and nanoclusters. Colloids Surfaces A Physicochem Eng Asp 2017;532:601–8. https://doi.org/10.1016/j.colsurfa.2017.02.047.
[40] Ungor D, Csapó E, Kismárton B, Juhász A, Dékány I. Nucleotide-directed syntheses of gold nanohybrid systems with structure-dependent optical features: selective fluorescence sensing of Fe3+ ions. Colloids Surf B: Biointerfaces 2017;155:135–41. https://doi.org/10.1016/j.colsurfb.2017.04.013.
[41] Ungor D, Szilágyi I, Csapó E. Yellow-emitting Au/Ag bimetallic nanoclusters with high photostability for detection of folic acid. J Mol Liq 2021;338:116695. https://doi.org/10.1016/j.molliq.2021.116695.
[42] Hornok V, Csapó E, Varga N, Ungor D, Sebők D, Janovák L, et al. Controlled syntheses and structural characterization of plasmonic and red-emitting gold/lysozyme nanohybrid dispersions. Colloid Polym Sci 2016;294:49–58. https://doi.org/10.1007/s00396-015-3781-7.
[43] Ungor D, Horváth K, Dékány I, Csapó E. Red-emitting gold nanoclusters for rapid fluorescence sensing of tryptophan metabolites. Sensors Actuators B Chem 2019;288:728–33. https://doi.org/10.1016/j.snb.2019.03.026.
[44] Al Kindi H, Mohamed A, Kajimoto S, Zhanpeisov N, Horino H, Shibata Y, et al. Single bovine serum albumin molecule can hold plural blue-emissive gold nanoclusters: A quantitative study with two-photon excitation. J Photochem Photobiol A Chem 2018;357:168–74. https://doi.org/10.1016/j.jphotochem.2018.02.029.
[45] Chevrier DM, Thanthirige VD, Luo Z, Driscoll S, Cho P, Macdonald MA, et al. Structure and formation of highly luminescent protein-stabilized gold clusters. Chem Sci 2018;9:2782–90. https://doi.org/10.1039/c7sc05086k.
[46] Hsu YC, Hung MJ, Chen YA, Wang TF, Ou YR, Chen SH. Identifying reducing and capping sites of protein-encapsulated gold nanoclusters. Molecules 2019;24:1–13. https://doi.org/10.3390/molecules24081630.
[47] Xu Y, Sherwood J, Qin Y, Crowley D, Bonizzoni M, Bao Y. The role of protein characteristics in the formation and fluorescence of Au nanoclusters. Nanoscale 2014;6:1515–24. https://doi.org/10.1039/c3nr06040c.
[48] Maity B, Abe S, Ueno T. Observation of gold sub-nanocluster nucleation within a crystalline protein cage. Nat Commun 2017;8. https://doi.org/10.1038/ncomms14820.
[49] Shang L, Brandholt S, Stockmar F, Trouillet V, Bruns M, Nienhaus GU. Effect of protein adsorption on the fluorescence of ultrasmall gold nanoclusters. Small 2012;8:661–5. https://doi.org/10.1002/smll.201101353.
[50] Shang L, Dörlich RM, Trouillet V, Bruns M, Nienhaus GU. Ultrasmall fluorescent silver nanoclusters: Protein adsorption and its effects on cellular responses. Nano Res 2012;5:531–42. https://doi.org/10.1007/s12274-012-0238-x.
[51] Shang L, Yang L, Seiter J, Heinle M, Brenner-Weiss G, Gerthsen D, et al. Nanoparticles Interacting with Proteins and Cells: A Systematic Study of Protein Surface Charge Effects. Adv Mater Interfaces 2014;1:1–10. https://doi.org/10.1002/admi.201300079.
[52] Shang L, Nienhaus GU. Metal nanoclusters: Protein corona formation and implications for biological applications. Int J Biochem Cell Biol 2016;75:175–9. https://doi.org/10.1016/j.biocel.2015.09.007.
[53] Shang L, Nienhaus GU. Research Update: Interfacing ultrasmall metal nanoclusters with biological systems. APL Mater 2017;5. https://doi.org/10.1063/1.4974514.
[54] Zheng C, Wang H, Xu W, Xu C, Liang J, Han H. Study on the interaction between histidine-capped Au nanoclusters and bovine serum albumin with spectroscopic techniques. Spectrochim Acta - Part A Mol Biomol Spectrosc 2014;118:897–902. https://doi.org/10.1016/j.saa.2013.09.082.
[55] Sahu DK, Sahu K. Characterizing optical properties, composition of stabilizer-free copper nanoclusters and its interaction with bovine serum albumin. J Photochem Photobiol A Chem 2017;347:17–25. https://doi.org/10.1016/j.jphotochem.2017.07.002.
[56] Wang Y, Zhang J, Huang L, He D, Ma L, Ouyang J, et al. Novel application of Ag nanoclusters in fluorescent imaging of human serum proteins after native polyacrylamide gel electrophoresis (PAGE). Chem - A Eur J 2012;18:1432–7. https://doi.org/10.1002/chem.201101310.
[57] Xu S, Lu X, Yao C, Huang F, Jiang H, Hua W, et al. A visual sensor array for pattern recognition analysis of proteins using novel blue-emitting fluorescent gold nanoclusters. Anal Chem 2014;86:11634–9. https://doi.org/10.1021/ac502643s.
[58] Yuan Z, Du Y, Tseng YT, Peng M, Cai N, He Y, et al. Fluorescent gold nanodots based sensor array for proteins discrimination. Anal Chem 2015;87:4253–9. https://doi.org/10.1021/ac5045302.
[59] Xu S, Wu Y, Sun X, Wang Z, Luo X. A multicoloured Au NCs based cross-reactive sensor array for discrimination of multiple proteins. J Mater Chem B 2017;5:4207–13. https://doi.org/10.1039/c7tb00367f.
[60] Deng HH, Shi XQ, Balasubramanian P, Huang KY, Xu YY, Huang ZN, et al. 6-Aza-2-thio-thymine stabilized gold nanoclusters as photoluminescent probe for protein detection. Nanomaterials 2020;10. https://doi.org/10.3390/nano10020281.
[61] Akhuli A, Chakraborty D, Agrawal AK, Sarkar M. Probing the interaction of bovine serum albumin with copper nanoclusters: realization of binding pathway different from protein corona. Langmuir 2021;37:1823–37. https://doi.org/10.1021/acs.langmuir.0c03176.
[62] Paramanik B, Kundu A, Chattopadhyay K, Patra A. Study of binding interactions between MPT63 protein and Au nanocluster. RSC Adv 2014;4:35059–66. https://doi.org/10.1039/c4ra03708a.
[63] Ye T, Li C, Su C, Ji X, He Z. Enzymatic synthesis of a DNA-templated alloy nanocluster and its application in a fluorescence immunoassay. RSC Adv 2015;5:55336–9. https://doi.org/10.1039/c5ra07509b.
[64] Maghsudi M, Shahabadi N, Kooshk MRA, Ghaemi N, Nemati L, Parvaneh S, et al. Nontoxic silver nanocluster-induced folding, fibrillation, and aggregation of blood plasma proteins. Int J Biol Macromol 2018;119:838–48. https://doi.org/10.1016/j.ijbiomac.2018.07.177.
[65] Jia XY, Xue YR, Zhang CX, Luo Q, Wu Y. Highly sensitive detection of the human papillomavirus E6 protein by DNA-protected silver nanoclusters and the intrinsic mechanism. New J Chem 2019;43:14944–51. https://doi.org/10.1039/c9nj03241j.
[66] Guo P, Sknepnek R. Olvera De La Cruz M. Electrostatic-driven ridge formation on nanoparticles coated with charged end-group ligands. J Phys Chem C 2011;115:6484–90. https://doi.org/10.1021/jp201598k.
[67] Lin JQ, Zheng YG, Zhang HW, Chen Z. A simulation study on nanoscale holes generated by gold nanoparticles on negative lipid bilayers. Langmuir 2011;27:8323–32. https://doi.org/10.1021/la201086u.
[68] Lee OS, Schatz GC. Computational simulations of the interaction of lipid membranes with DNA-functionalized gold nanoparticles. Methods Mol Biol 2011;726:283–96. https://doi.org/10.1007/978-1-61779-052-2_18.
[69] Brancolini G, Kokh DB, Calzolai L, Wade RC, Corni S. Docking of ubiquitin to gold nanoparticles. ACS Nano 2012;6:9863–78. https://doi.org/10.1021/nn303444b.
[70] An D, Su J, Weber JK, Gao X, Zhou R, Li J. A peptide-coated gold nanocluster exhibits unique behavior in protein activity inhibition. J Am Chem Soc 2015;137:8412–8. https://doi.org/10.1021/jacs.5b00888.
[71] Ramezani F, Rafii-Tabar H. An in-depth view of human serum albumin corona on gold nanoparticles. Mol BioSyst 2015;11:454–62. https://doi.org/10.1039/c4mb00591k.
[72] Tavanti F, Menziani MC. Computational insight on the interaction of common blood proteins with gold nanoparticles. Int J Mol Sci 2021;22. https://doi.org/10.3390/ijms22168722.
[73] Russell BA, Kubiak-Ossowska K, Mulheran PA, Birch DJS, Chen Y. Locating the nucleation sites for protein encapsulated gold nanoclusters: A molecular dynamics and fluorescence study. Phys Chem Chem Phys 2015;17:21935–41. https://doi.org/10.1039/c5cp02380g.
[74] Boulos SP, Davis TA, Yang JA, Lohse SE, Alkilany AM, Holland LA, et al. Nanoparticle-protein interactions: A thermodynamic and kinetic study of the adsorption of bovine serum albumin to gold nanoparticle surfaces. Langmuir 2013;29:14984–96. https://doi.org/10.1021/la402920f.
[75] Davidson AM, Brust M, Cooper DL, Volk M. Sensitive analysis of protein adsorption to colloidal gold by differential centrifugal sedimentation. Anal Chem 2017;89:6807–14. https://doi.org/10.1021/acs.analchem.7b01229.
[76] Luan Y, Li D, Wang Y, Liu X, Brash JL, Chen H. 125I-radiolabeling, surface plasmon resonance, and quartz crystal microbalance with dissipation: Three tools to compare protein adsorption on surfaces of different wettability. Langmuir 2014;30:1029–35. https://doi.org/10.1021/la403498w.
[77] Zhang H, Huang J, Wang Y, Liu R, Huai X, Jiang J, et al. Atomic force microscopy for two-dimensional materials: A tutorial review. Opt Commun 2018;406:3–17. https://doi.org/10.1016/j.optcom.2017.05.015.
[78] Kovács AN, Varga N, Juhász Á, Csapó E. Serum protein-hyaluronic acid complex nanocarriers: structural characterisation and encapsulation possibilities. Carbohydr Polym 2021;251:117047. https://doi.org/10.1016/j.carbpol.2020.117047.

[79] Juhász Á, Csapó E, Vécsei L, Dékány I. Modelling and characterization of the sorption of kynurenic acid on protein surfaces. Period Polytech Chem Eng 2017; 61:3–9. https://doi.org/10.3311/PPch.10185.
[80] Wasilewska M, Adamczyk Z, Pomorska A, Nattich-Rak M, Sadowska M. Human serum albumin adsorption kinetics on silica: influence of protein solution stability. Langmuir 2019;35:2639–48. https://doi.org/10.1021/acs.langmuir.8b03266.
[81] Adamczyk Z. Protein adsorption: A quest for a universal mechanism. Curr Opin Colloid Interface Sci 2019;41:50–65. https://doi.org/10.1016/j.cocis.2018.11.004.
[82] Bratek-Skicki A, Sadowska M, Maciejewska-Prończuk J, Adamczyk Z. Nanoparticle and bioparticle deposition kinetics: Quartz microbalance measurements. Nanomaterials 2021;11:1–42. https://doi.org/10.3390/nano11010145.
[83] Ying P, Yu Y, Jin G, Tao Z. Competitive protein adsorption studied with atomic force microscopy and imaging ellipsometry. Colloids Surf B: Biointerfaces 2003; 32:1–10. https://doi.org/10.1016/S0927-7765(02)00133-9.
[84] Servoli E, Maniglio D, Aguilar MR, Motta A, San Roman J, Belfiore LA, et al. Quantitative analysis of protein adsorption via atomic force microscopy and surface plasmon resonance. Macromol Biosci 2008;8:1126–34. https://doi.org/10.1002/mabi.200800110.
[85] Pasche Stéphanie, Susan M, Paul De, Vörös Janos, Spencer Nicholas D, Textor M. Poly(l-lysine)-graft-poly(ethylene glycol) Assembled Monolayers on Niobium Oxide Surfaces:A Quantitative Study of the Influence of Polymer Interfacial Architecture on Resistance to Protein Adsorption by ToF-SIMS and in Situ OWLS. Langmuir 2003;19:9216–25. https://doi.org/10.1021/LA034111Y.
[86] Hook FF, Vörös J, Rodahl M, Kurrat R, Böni P, Ramsden JJ, et al. A comparative study of protein adsorption on titanium oxide surfaces using in situ ellipsometry, optical waveguide lightmode spectroscopy, and quartz crystal microbalance/dissipation. Colloids Surf B: Biointerfaces 2002;24:155–70. https://doi.org/10.1016/S0927-7765(01)00236-3.
[87] Saftics A, Prósz GA, Türk B, Peter B, Kurunczi S, Horvath R. In situ viscoelastic properties and chain conformations of heavily hydrated carboxymethyl dextran layers: a comparative study using OWLS and QCM-I chips coated with waveguide material. Sci Rep 2018;8:1–14. https://doi.org/10.1038/s41598-018-30201-6.
[88] Vörös J. The density and refractive index of adsorbing protein layers. Biophys J 2004;87:553–61. https://doi.org/10.1529/biophysj.103.030072.
[89] Lori JA, Hanawa T. Adsorption characteristics of albumin on gold and titanium metals in Hanks' solution using EQCM. Spectroscopy 2004;18:545–52. https://doi.org/10.1155/2004/834639.
[90] Csapó E, Juhász Varga N, Sebők D, Hornok V, Janovák L, et al. Thermodynamic and kinetic characterization of pH-dependent interactions between bovine serum albumin and ibuprofen in 2D and 3D systems. Colloids Surfaces A Physicochem Eng Asp 2016;504:471–8. https://doi.org/10.1016/j.colsurfa.2016.05.090.
[91] Adamczyk Z, Pomorska A, Nattich-Rak M, Wytrwal-Sarna M, Bernasik A. Protein adsorption mechanisms at rough surfaces: Serum albumin at a gold substrate. J Colloid Interface Sci 2018;530:631–41. https://doi.org/10.1016/j.jcis.2018.06.063.
[92] Pomorska A, Adamczyk Z, Nattich-Rak M, Sadowska M. Kinetics of human serum albumin adsorption at silica sensor: Unveiling dynamic hydration function. Colloids Surf B: Biointerfaces 2018;167:377–84. https://doi.org/10.1016/j.colsurfb.2018.04.017.
[93] Thourson SB, Marsh CA, Doyle BJ, Timpe SJ. Quartz crystal microbalance study of bovine serum albumin adsorption onto self-assembled monolayer-functionalized gold with subsequent ligand binding. Colloids Surf B: Biointerfaces 2013;111:707–12. https://doi.org/10.1016/j.colsurfb.2013.06.053.
[94] Varga N, Csapó E, Majláth Z, Ilisz I, Krizbai IA, Wilhelm I, et al. Targeting of the kynurenic acid across the blood–brain barrier by core-shell nanoparticles. Eur J Pharm Sci 2016;86:67–74.
[95] Beykal B, Herzberg M, Oren Y, Mauter MS. Influence of surface charge on the rate, extent, and structure of adsorbed Bovine Serum Albumin to gold electrodes. J Colloid Interface Sci 2015;460:321–8. https://doi.org/10.1016/j.jcis.2015.08.055.
[96] Homola J, Yee SS, Gauglitz G. Surface plasmon resonance sensors: review. Sensors Actuators B Chem 1999;54:3–15. https://doi.org/10.1016/S0925-4005(98)00321-9.
[97] Homola J. Surface plasmon resonance sensors for detection of chemical and biological species. Chem Rev 2008;108:462–93. https://doi.org/10.1021/cr068107d.
[98] Rüger F, Keusgen M, Vornicescu D. Gold albumin sandwich structures for enhanced biosensing using surface plasmon resonance. Phys Status Solidi Appl Mater Sci 2021;218:2100029. https://doi.org/10.1002/pssa.202100029.
[99] Wang J, Zhou HS. Aptamer-based Au nanoparticles-enhanced surface plasmon resonance detection of small molecules. Anal Chem 2008;80:7174–8. https://doi.org/10.1021/ac801281c.
[100] Melaine F, Roupioz Y, Buhot A. Gold nanoparticles surface plasmon resonance enhanced signal for the detection of small molecules on split-aptamer microarrays (small molecules detection from split-aptamers). Microarrays 2015;4:41–52. https://doi.org/10.3390/microarrays4010041.
[101] Luo Z, Zhang J, Wang Y, Chen J, Li Y, Duan Y. An aptamer based method for small molecules detection through monitoring salt-induced AuNPs aggregation and surface plasmon resonance (SPR) detection. Sensors Actuators B Chem 2016;236:474–9. https://doi.org/10.1016/j.snb.2016.06.035.
[102] Wang H, Wang X, Wang J, Fu W, Yao C. A SPR biosensor based on signal amplification using antibody-QD conjugates for quantitative determination of multiple tumor markers. Sci Rep 2016;6:1–9. https://doi.org/10.1038/srep33140.
[103] Hutter E, Cha S, Liu JF, Park J, Yi J, Fendler JH, et al. Role of substrate metal in gold nanoparticle enhanced surface plasmon resonance imaging. J Phys Chem B 2001;105:8–12. https://doi.org/10.1021/jp003565q.
[104] Hong X, Hall EAH. Contribution of gold nanoparticles to the signal amplification in surface plasmon resonance. Analyst 2012;137:4712–9. https://doi.org/10.1039/c2an35742a.
[105] Usman F, Dennis JO, Seong KC, Ahmed AY, Ferrell TL, Fen YW, et al. Enhanced sensitivity of surface plasmon resonance biosensor functionalized with doped polyaniline composites for the detection of low-concentration acetone vapour. J Sensors 2019:2019. https://doi.org/10.1155/2019/5786105.
[106] Sim HR, Wark AW, Lee HJ. Attomolar detection of protein biomarkers using biofunctionalized gold nanorods with surface plasmon resonance. Analyst 2010; 135:2528–32. https://doi.org/10.1039/c0an00457j.
[107] Kim S, Lee S, Lee HJ. An aptamer-aptamer sandwich assay with nanorod-enhanced surface plasmon resonance for attomolar concentration of norovirus capsid protein. Sensors Actuators B Chem 2018;273:1029–36. https://doi.org/10.1016/j.snb.2018.06.108.
[108] Constantin E, Varasteanu P, Mihalache I, Tutunaru O, Popescu M, Boldeiu A, et al. Femtomolar SPR detection of protein enhanced by seedless synthesized gold nanorods. SSRN Electron J 2021. https://doi.org/10.2139/ssrn.3844711.
[109] Wu Q, Sun Y, Ma P, Zhang D, Li S, Wang X, et al. Gold nanostar-enhanced surface plasmon resonance biosensor based on carboxyl-functionalized graphene oxide. Anal Chim Acta 2016;913:137–44. https://doi.org/10.1016/j.aca.2016.01.063.
[110] Kwon MJ, Lee J, Wark AW, Lee HJ. Nanoparticle-enhanced surface plasmon resonance detection of proteins at attomolar concentrations: Comparing different nanoparticle shapes and sizes. Anal Chem 2012;84:1702–7. https://doi.org/10.1021/ac202957h.